Inverse Scattering Using a Kohn-Vogelius Formulation and Shape Optimization Method

Thomas Bonnafont*, Fabien Caubet†,

*Lab-STICC, UMR CNRS 6285, ENSTA Bretagne, 29806 Brest, France, thomas.bonnafont@ensta-bretagne.fr
†E2S UPPA, CNRS, LMAP, UMR 5142, 64000 Pau, France, fabien.caubet@univ-pau.fr

Abstract—This paper presents a method to retrieve the form of a metallic object given partial electromagnetic measurements. We propose a numerical resolution of this inverse problem based on a shape optimization method. More precisely, we aim to minimize the so-called Kohn-Vogelius functional, which is numerically more stable than the least squares functional, by computing its shape gradient. The optimization problem is then solved using a Nesterov inertial scheme to accelerate the descent algorithm. Numerical simulations in 2D are provided to highlight the efficiency of the proposed method.

Index Terms—Inverse scattering, Shape optimization, Kohn-Vogelius functional, Nesterov scheme.

I. INTRODUCTION

In this article, we are interested in the electromagnetic inverse scattering problem, e.g. retrieving the shape of an object from radar cross-section measurements. In this context, many inversion techniques have been developed, see, e.g., [1], [2], [3], [4].

One can think for example of inverse synthetic-aperture radar techniques, where the movement of the targets (or the emitter) is used in order to obtain an image of the target [5], [6]. Indeed, the movements introduce a Doppler effect that helps to construct a high-resolution image of the object using signal theory techniques.

Since the 90's in acoustics (see, e.g., [7], [8], [9], [10]) and the early 00's in electromagnetic (see, e.g., [1], [2], [3]), the shape optimization methodology has received increasing attention. Indeed, the main difference is that with this technique no movements are needed to retrieve the shape of the target. The main results have been obtained using either topological (as in [9]) or level-set (as in [2], [10]) methods and by considering mainly a least squares based cost functional. Furthermore, both methods allow to retrieve complicated shapes and multiple targets (see, e.g., [9], [2]). Besides, the choice of the least squares functional is straightforward since the method of moments (see [11]) is widely used to compute the scattered field at a certain distance for complicated object shapes. In those methods, after the calculation of the shape gradient, conventional gradient descent schemes are used to minimize the cost functional. Recently, the Nesterov accelerated gradient descent has been introduced in the context of shape optimization for acoustic inverse scattering problems in [10].

Nevertheless, in the shape optimization community, it has been shown that another functional is more robust and numerically stable than the least squares one: the Kohn-Vogelius

functional, used for example in [12]. This latter has been used in particular for detecting objects immersed in fluids in [13], where stability is very important. However, this latter needs to compute the field over the whole domain, instead of only on its boundary. With the rise of fast computational methods for electromagnetic propagation (see, e.g., [14]) and the enhancement of computer speed, this latter becomes less of a burden.

Therefore, in this article, we are interested in introducing the Kohn-Vogelius formulation to the electromagnetic inverse scattering problem. Furthermore, a Nesterov accelerated gradient descent is used to solve the optimization problem.

The remaining of the article is organized as follows. Section II introduces the notation, the forward problem, and the inverse problem we are interested in. Section III focuses on the shape optimization-based inversion technique using the Kohn-Vogelius cost functional. Section IV is dedicated to the numerical tests and highlights the advantages of the proposed formulation. Section V concludes the paper and gives perspectives for future works.

II. THE INVERSE PROBLEM

A. Notations

Let us begin by introducing the notations used in this paper. We point out that the vectors are denoted in bold, such as $\boldsymbol{V}$. In the following, Ω denotes a non-empty bounded open set of $\mathbb{R}^2$, with a boundary $\partial\Omega$. The exterior unit normal to $\partial\Omega$ is denoted by $\mathbf{n}$, and, for a smooth function u, the normal derivative is $\partial_n u = \nabla u \cdot \mathbf{n}$. For a given complex number z, we denote by $\Re(z)$ its real part, by $\Im(z)$ its imaginary part, and by $\bar{z}$ its complex conjugate. The imaginary unit is denoted by j and a $\exp(j\omega t)$ time dependence is assumed in this work, where ω is the angular frequency. The frequency is denoted by f, and $k = \frac{2\pi f}{c}$ corresponds to the wave number, where c is the speed of light. Besides, the Cartesian coordinates system (x, y) is used hereafter.

We here consider the scattering of a given Perfectly Metallic Conductor (PEC), denoted by $\mathcal{O}$ with a smooth boundary $\partial\mathcal{O}$, strictly included in the domain Ω. We assume that in $\Omega\backslash\overline{\mathcal{O}}$, the permittivity and the permeability are respectively given by $\varepsilon = \varepsilon_0$ and $\mu = \mu_0$: it corresponds to the free-space. Moreover we assume that $\partial\Omega$ is divided into two non empty open sub-domains Γ_m and Γ_c such that $\overline{\Gamma_m \cup \Gamma_c} = \partial\Omega$ and $\Gamma_m \cap \Gamma_c = \emptyset$ (Γ_m will represent the subset where the measurements are made and Γ_c is its complement). Both sub-domains are not

necessarily connected and can then consist of multiple pieces. The incident and scattered waves are denoted by u_i and u_s, respectively. The incident wave is assumed to be a plane wave with an angle of incidence from the x-axis denoted by θ_i, and an amplitude of u_{i_0}. The total field u corresponds to the sum of both such that

$$u = u_\mathrm{i} + u_\mathrm{s}.$$

The notations are pictured in Fig. 1, with the target $\mathcal{O}$ in red.
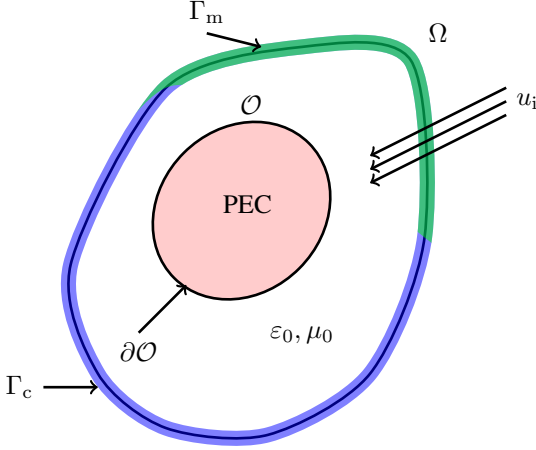

Fig. 1. Example of the considered domain Ω with the scatterer $\mathcal{O}$ (in red) inside.

B. The considered inverse obstacle problem

Since the object is considered to be a PEC, the mathematical formulation of the forward problem is as follows

$$\begin{cases} \Delta u + k^2 u &= 0 \quad \text{in } \Omega\backslash\overline{\mathcal{O}}, \\ \partial_\mathrm{n} u + jku &= h \quad \text{on } \partial\Omega, \\ u &= 0 \quad \text{on } \partial\mathcal{O}. \end{cases} \quad (1)$$

In this problem, we define

$$h = j(k - \mathbf{k}_\mathrm{i}(\theta_\mathrm{i}) \cdot \mathbf{n}) u_{\mathrm{i}_0} \exp(-j\mathbf{k}_\mathrm{i}(\theta_\mathrm{i}) \cdot \mathbf{r}),$$

where $\mathbf{k}_\mathrm{i}$ corresponds to the incident wave vector given by

$$\mathbf{k}_\mathrm{i} = -k \left(\cos(\theta_\mathrm{i}), \sin(\theta_\mathrm{i}) \right),$$

and $\mathbf{r} = (x_M, y_M)$ is the position of a point $M \in \Omega$. This problem corresponds to the bounded formulation of the open scattering problem, where the boundary condition on $\partial\Omega$ is an absorbing boundary condition introduced such that the field respects the Sommerfeld condition.

The aim of this work is to numerically solve the corresponding inverse obstacle problem, from boundary measurements. More precisely, we assume that the measurements $u = g$ is known on Γ_m and we want to reconstruct the PEC $\mathcal{O}$. Thus, the inverse problem can be formulated as

Find $\mathcal{O}$ and the solution $u \in \mathrm{H}^1(\Omega\backslash\overline{\mathcal{O}})$ such that
$$\begin{cases} \Delta u + k^2 u &= 0 \quad \text{in } \Omega\backslash\overline{\mathcal{O}}, \\ \partial_\mathrm{n} u + jku &= h \quad \text{on } \Gamma_\mathrm{c}, \\ u &= 0 \quad \text{on } \partial\mathcal{O}, \\ \partial_\mathrm{n} u &= \tilde{h} \quad \text{on } \Gamma_\mathrm{m}, \\ u &= g \quad \text{on } \Gamma_\mathrm{m}, \end{cases}$$

where $\tilde{h}$ is defined by

$$\tilde{h} = h - jkg.$$

III. A SHAPE OPTIMIZATION METHOD

A. Kohn-Vogelius formulation

In order to numerically solve the above inverse problem, a first classical idea would be to consider the minimization of a least squares cost functional as

$$\mathcal{J}(\mathcal{O}) = \frac{1}{2} \int_{\Gamma_\mathrm{m}} |u - g|^2,$$

where g is the measured field and u is the computed field solution of (1). This latter has the advantage of having a field u that is only computed on Γ_m. By defining an adjoint problem, the so-called *shape gradient* is computed and the gradient descent method can be used to reconstruct an approximation of $\mathcal{O}$. This is a classical approach in the literature, e.g., in [1], [2], [3], [10].

Here we propose to consider the minimization of a Kohn-Vogelius type functional, more stable, and efficient in practice (see, e.g., [12], [13]). The considered Kohn-Vogelius functional is defined as

$$\mathcal{K}(\mathcal{O}) = \frac{1}{2} \int_{\Omega\backslash\overline{\mathcal{O}}} |\nabla(u_\mathrm{D} - u_\mathrm{N})|^2, \quad (2)$$

where u_D is the unique solution to the following boundary problem

$$\begin{cases} \Delta u_\mathrm{D} + k^2 u_\mathrm{D} &= 0 \quad \text{in } \Omega\backslash\overline{\mathcal{O}}, \\ \partial_\mathrm{n} u_\mathrm{D} + jku_\mathrm{D} &= h \quad \text{on } \Gamma_\mathrm{c}, \\ u_\mathrm{D} &= g \quad \text{on } \Gamma_\mathrm{m}, \\ u_\mathrm{D} &= 0 \quad \text{on } \partial\mathcal{O}, \end{cases} \quad (3)$$

and u_N is the unique solution to the following boundary problem

$$\begin{cases} \Delta u_\mathrm{N} + k^2 u_\mathrm{N} &= 0 \quad \text{in } \Omega\backslash\overline{\mathcal{O}}, \\ \partial_\mathrm{n} u_\mathrm{N} + jku_\mathrm{N} &= h \quad \text{on } \Gamma_\mathrm{c}, \\ \partial_\mathrm{n} u_\mathrm{N} &= \tilde{h} \quad \text{on } \Gamma_\mathrm{m}, \\ u_\mathrm{N} &= 0 \quad \text{on } \partial\mathcal{O}. \end{cases} \quad (4)$$

It should be noted that if $\mathcal{O}$ is solution to the inverse problem (with an associated field u), then $u = u_\mathrm{D} = u_\mathrm{N}$ and then $\mathcal{O}$ is obviously a minimizer of $\mathcal{K}$. Conversely, if $\mathcal{O}$ is a minimizer of $\mathcal{K}$ and if we assume that the minimum is zero, then $u_\mathrm{D} = u_\mathrm{N}$, then the couple $(\mathcal{O}, u_\mathrm{D})$ is solution to the inverse problem. For these reasons, it is reasonable to consider the minimization of $\mathcal{K}$ in order to solve the original inverse problem.

B. Shape gradient computation

In order to minimize the above Kohn-Vogelius functional, we will compute its shape gradient. Roughly speaking, the shape gradient of $\mathcal{K}$ at $\mathcal{O}$ is obtained by computing $\lim_{t\to 0} \dfrac{\mathcal{K}(\mathcal{O}_t) - \mathcal{K}(\mathcal{O})}{t}$, where $\mathcal{O}_t = (\mathbf{I} + t\boldsymbol{V})(\mathcal{O})$ is a perturbation of the domain $\mathcal{O}$, with $t \neq 0$ and $\boldsymbol{V}$ a direction perturbation (see, e.g., [15], [16] for details on the notion of shape derivatives). It is well-known from a structural result

(see, e.g., [15, Theorem 5.9.2]) that the shape gradient can be expressed as

$$\nabla \mathcal{K}(\mathcal{O}) \cdot \boldsymbol{V} = \int_{\partial \mathcal{O}} \varphi(\mathcal{O}) \left(\boldsymbol{V} \cdot \mathbf{n} \right),$$

where φ is a function independent of $\boldsymbol{V}$ but which may depend on the considered forward problems and some adjoint problems. This means that only the modifications on the geometry along the normal of the shape have effects on the cost functional. Note that results on the existence of the shape derivatives concerning our problem have been proven in [1].

In order to compute the shape gradient, we introduce the solutions w and z to the respective two following adjoint problems

$$\begin{cases} \Delta w + k^2 w &= -k^2 (\overline{u_D - u_N}) & \text{in } \Omega \backslash \overline{\mathcal{O}}, \\ \partial_n w + jkw &= -jk(\overline{u_D - u_N}) & \text{on } \Gamma_c, \\ \partial_n w &= 0 & \text{on } \Gamma_m, \\ w &= 0 & \text{on } \partial \mathcal{O}, \end{cases} \quad (5)$$

and

$$\begin{cases} \Delta z + k^2 z &= -k^2(\overline{u_D - u_N}) & \text{in } \Omega \backslash \overline{\mathcal{O}}, \\ \partial_n z + jkz &= \partial_n (\overline{u_D - u_N}) & \text{on } \Gamma_c, \\ z &= 0 & \text{on } \Gamma_m, \\ z &= 0 & \text{on } \partial \mathcal{O}. \end{cases} \quad (6)$$

In a few words, the first one allows putting to 0 the integral over Neumann boundaries in the calculation of the shape derivative, while the second one sets to 0 the Dirichlet ones. Using u_D, u_N, w and z solutions to Problems (3), (4), (5) and (6), the shape gradient can be expressed as

$$\nabla K(\mathcal{O}) \cdot \boldsymbol{V} = \Re \left(\int_{\partial \mathcal{O}} \left(\partial_n u_D \left(\partial_n z - \partial_n(\overline{u_D - u_N}) \right) - \right. \right.$$
$$\left. \left. \partial_n w \partial_n u_N + \frac{1}{2} |\nabla(u_D - u_N)|^2 \right) (\boldsymbol{V} \cdot \mathbf{n}) \right). \quad (7)$$

Notice that, in order to compute its shape gradient, we have to solve, at each iteration, four partial differential equations of the same type. Indeed, only the source term is different, thus it is not too expensive numerically. If we consider the least squares based functional, only two problems have to be solved (a forward and an adjoint problem). However, the main advantage of this approach is that we obtain better robustness and numerical stability.

C. Numerical inversion strategy

From now on, the aim is to numerically minimize the Kohn-Vogelius functional (2), that is to approach the solution to the following optimization problem

$$\min_{\mathcal{O} \in \mathcal{U}_{ad}} \mathcal{K}(\mathcal{O}),$$

on a set $\mathcal{U}_{ad}$ of admissible shapes. Here we consider a truncated Fourier series parametrization for the boundary of

the object $\mathcal{O}$. Thus, the optimization works on each of the Fourier coefficients, such that

$$\partial \mathcal{O} = \Big\{ (x_c, y_c)^t + r(\cos(\Theta), \sin(\Theta))^t$$
$$+ \sum_{n \geq 1}^{N} (a_n, b_n)(\cos(n\Theta), \sin(n\Theta))^t (\cos(\Theta), \sin(\Theta))^t,$$
$$\Theta \in [0, 2\pi[\Big\},$$

where the upper script ^{t} denotes the transpose, (x_c, y_c) is the center, r is the radius, and where $N \in \mathbb{N}^*$.

To solve this numerical problem, we have performed a Nesterov gradient descent scheme with restart (see [17] for details on the algorithm), using the shape gradient given by (7). Indeed, the Nesterov gradient descent method allows being faster than the usual gradient descent, since the step is modified along the optimization process. In a few words, if the usual gradient scheme can be seen as the descent of the ball along a curve, here the speed of the ball is modified along by accelerating it using a weighted combination of the previous iterations, introducing a kind of inertia during the descent process. Nevertheless, one problem is that, by increasing the speed of convergence, one can go beyond the minimum and increase the cost functional. Thus, a restart strategy is introduced to overcome this problem.

Moreover, for better stability, we precise that the Fourier coefficients are added one after another, after a given number of iterations. More precisely, we first search for the center of the object during a small number of iterations, then the radius is also changed, and after that the coefficients are added one after the other after N_p iterations. The initial guess $\mathcal{O}_0$ is a circle of center (x_{c_0}, y_{c_0}) and radius r_0.

IV. NUMERICAL TESTS

In this part, some numerical tests are performed on two different shapes: an ellipse and a more complex one. In all those tests, the different problems are solved using FreeFem++ (see [18]), which is a finite element based solver. For those tests, artificial data are computed from the direct problem (1) using a P2 finite element strategy on a coarse mesh. In order to avoid the so-called *inverse crime*, Problems (3), (4), (5) and (6), needed for the inversion strategy, are solved using the P1 finite elements on a less coarse mesh. Also, the results obtained with a least squares based cost functional are provided for comparison.

A. Retrieving an ellipse

In this test, we aim to retrieve the ellipse provided in Fig. 2, in plain line, i.e. its center, and both radii. The initial guess is the circle pictured in Fig. 2, in red dotted line. The domain Ω is a square and the measurements are performed on the top, bottom, and right boundaries of Ω, pictured in green in Fig. 2. The incident field u_i is coming from $\theta_i = 90°$, with a frequency of 3 MHz. The number of iterations for the inversion strategy is here fixed to 400. One could also adjust a stopping criterion on the accuracy of the results. Here the

center is searched for 5 iterations, then the radius is modified, and after a Fourier mode is added each $N_p = 75$ iterations.

In Fig. 2, we plot the obtained shapes, in orange dotted lines, with both the least squares functional in Fig. 2(a) and the proposed Kohn-Vogelius formulation in Fig. 2(b). In both cases, the ellipse is well retrieved. Nevertheless, one can see that the results with Kohn-Vogelius are a little bit better, in particular at the bottom of the ellipse.
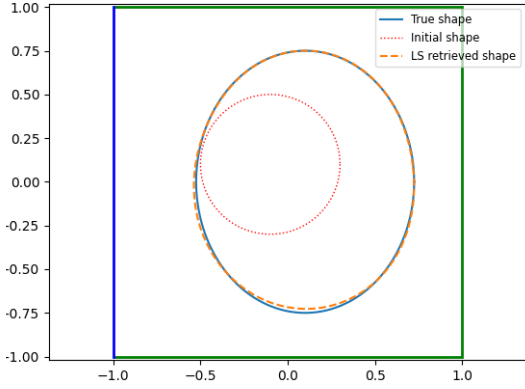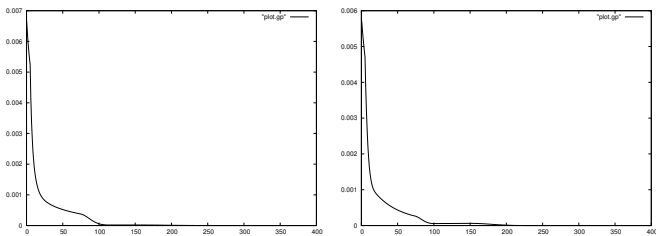

(a) Real and retrieved objects with the least squares cost functional
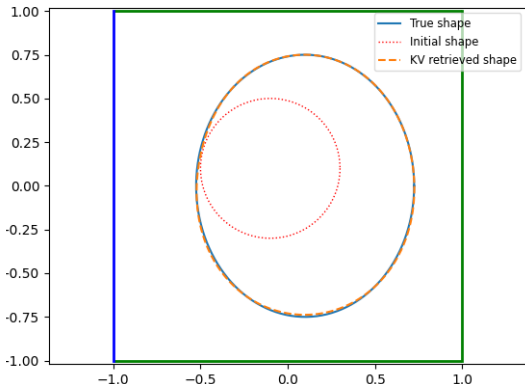
(b) Real and retrieved objects with the Kohn-Vogelius functional

Fig. 2. Real and approximated objects superposed.

For a better comparison, in Fig. 3, we plot the convergence of both the least squares and the Kohn-Vogelius functionals.

(a) Least squares cost functional con-   (b) Kohn-Vogelius cost functional con-
vergence   vergence

Fig. 3. Evolution of both cost functionals with the number of iterations.

As expected for this simple shape, both methods rapidly converge toward the results. After 100 iterations, the cost functional is below 10^{-4}.

B. Retrieving a more complex object

In this second test, we are looking for a more complex shape $\mathcal{O}$ with a convexity, i.e. more Fourier parameters to retrieve, and then some numerical instability in the reconstruction can be expected. The initial guess $\mathcal{O}_0$ is still a circle. Both the real shape and the initial guess are provided in Fig. 4, in plain and red dotted lines, respectively. As before, the domain Ω is a square, and measurements are performed on the top, bottom, and right boundary of Ω, pictured in green. The initial field is a plane wave coming from $\theta_i = 45°$, with a frequency of 3 MHz. Here, the total number of iterations is set up to 200. As previously, for 5 iterations, we only search for the center of $\mathcal{O}$ and then the radius is modified. After that, each $N_p = 15$ iterations, a Fourier mode is added to the search space.

In Fig. 4, the final obtained shape with both the least squares, in Fig. 4(a), and the Kohn-Vogelius, in Fig. 4(b), functionals are plotted in orange dotted lines.
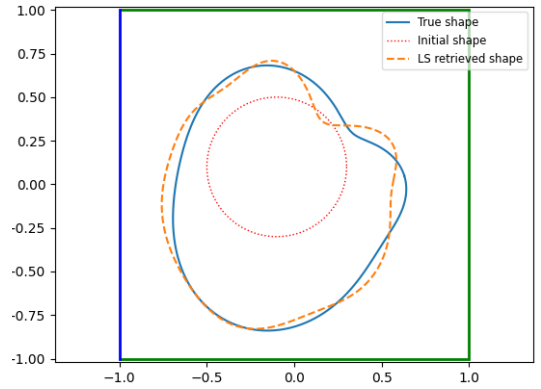
(a) Approximated object with least squares based shape inversion
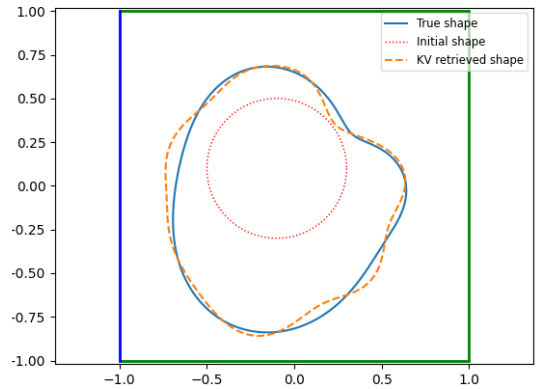
(b) Retrieved object with Kohn-Vogelius based shape inversion

Fig. 4. Real and obtained objects superposed for both cost functionals.

Here, we can see that the Kohn-Vogelius formulation outperforms the least squares one. Indeed, after 200 iterations with the Kohn-Vogelius functional, we retrieve almost exactly

the object $\mathcal{O}$, while with the least squares one, the convex part is not well retrieved. In both cases, the error at the bottom is due to the fact that no measurements are performed on the left side of the domain, and also since the field comes from the upper right corner. However, this configuration leads to a better approximation of the convex part.

To conclude on this test, we plot in Fig. 5 the convergence of both functionals.
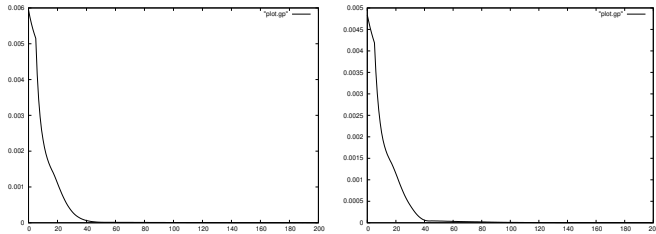
(a) Least squares functional conver-(b) Kohn-Vogelius functional conver-gence   gence

Fig. 5. Evolution of the least squares, in (a), and Kohn-Vogelius functionals with respect to the number of iterations.

In Fig. 5, we can see that both methods converge in almost 40 iterations here. Nevertheless, the results with the Kohn-Vogelius formulation are more precise, the error is almost half the one obtained with the least squares cost functional. This latter was also seen with the retrieved objects. Therefore, this test shows the advantage of the proposed formulation, when aiming at retrieving complex objects.

V. Conclusion and future works

In this work, a shape optimization procedure is used for the inverse scattering problem. To obtain better robustness and numerical stability, a Kohn-Vogelius cost functional has been introduced, in place of the widely used least squares functional. The shape gradient for this function has been derived, by introducing some appropriate adjoint problems. This shape gradient is then used to solve the derived minimization problem with a Nesterov accelerated gradient method with restart.

Numerical tests have been performed on different shapes. The Kohn-Vogelius formulation outperforms the least squares functional in terms of accuracy and thus in terms of convergence for a given error, especially in the case of complex geometries. Nevertheless, this comes at a price on the computation time, since twice as many more problems need to be solved. Nevertheless, the problems are of the same type, with only the source term being different, allowing efficient numerical implementation.

In forthcoming work, in order to be more accurate in terms of models, we will consider multiple sources and receptors (e.g. antenna array, or a moving antenna in an anechoic chamber). This should also improve the accuracy of the reconstruction since different measures will be available. We also aim to include a robust shape retrieval method with respect to the noise on the measurements, following the work [17]. Finally, we are also investigating the introduction of different media to account for more realistic environments and objects.

References

[1] A. Litman, D. Lesselier, and F. Santosa, "Reconstruction of a two-dimensional binary obstacle by controlled evolution of a level-set," *Inverse Problems*, vol. 14, pp. 685–706, June 1998.

[2] O. Dorn and D. Lesselier, "Level set methods for inverse scattering," *Inverse Problems*, vol. 22, pp. R67–R131, Aug. 2006.

[3] M. Benedetti, D. Lesselier, M. Lambert, and A. Massa, "A multi-resolution technique based on shape optimization for the reconstruction of homogeneous dielectric objects," *Inverse Problems*, vol. 25, p. 015009, Jan. 2009.

[4] P. Rocca, M. Benedetti, M. Donelli, D. Franceschini, and A. Massa, "Evolutionary optimization as applied to inverse scattering problems," *Inverse Problems*, vol. 25, p. 123003, Nov. 2009. Publisher: IOP Publishing.

[5] M. Prickett and C. Chen, "Principles of inverse synthetic aperture radar/isar/imaging," in *EASCON'80; Electronics and Aerospace Systems Conference*, pp. 340–345, 1980.

[6] F. Comblet, A. Khenchaf, A. Baussard, and F. Pellen, "Bistatic synthetic aperture radar imaging: Theory, simulations, and validations," *IEEE Transactions on Antennas and Propagation*, vol. 54, no. 11, pp. 3529–3540, 2006.

[7] G. Crosta, "A Shape Optimization Problem in Inverse Acoustics," in *Control and Optimal Design of Distributed Parameter Systems* (A. Friedman, W. Miller, J. E. Lagnese, D. L. Russell, and L. W. White, eds.), vol. 70, pp. 1–23, New York, NY: Springer New York, 1995. Series Title: The IMA Volumes in Mathematics and its Applications.

[8] G. R. Feijóo, A. A. Oberai, and P. M. Pinsky, "An application of shape optimization in the solution of inverse acoustic scattering problems," *Inverse Problems*, vol. 20, pp. 199–228, Dec. 2003. Publisher: IOP Publishing.

[9] G. R. Feijoo, "A new method in inverse scattering based on the topological derivative," *Inverse Problems*, vol. 20, pp. 1819–1840, Dec. 2004.

[10] L. Audibert, H. Haddar, and X. Liu, "An accelerated level-set method for inverse scattering problems," *SIAM Journal on Imaging Sciences*, vol. 15, no. 3, pp. 1576–1600, 2022.

[11] W. C. Gibson, *The method of moments in electromagnetics*. Chapman and Hall/CRC, 2021.

[12] L. Afraites, M. Dambrine, K. Eppler, and D. Kateb, "Detecting perfectly insulated obstacles by shape optimization techniques of order two," *Discrete & Continuous Dynamical Systems-B*, vol. 8, no. 2, p. 389, 2007.

[13] F. Caubet, M. Dambrine, D. Kateb, and C. Z. Timimoun, "A Kohn-Vogelius formulation to detect an obstacle immersed in a fluid," *Inverse Problems & Imaging*, vol. 7, no. 1, p. 123, 2013.

[14] M.-L. Yang, R.-Q. Liu, H.-W. Gao, and X.-Q. Sheng, "On the $\mathcal{H}$-LU-based fast finite element direct solver for 3-d scattering problems," *IEEE Transactions on Antennas and Propagation*, vol. 66, no. 7, pp. 3792–3797, 2018.

[15] A. Henrot and M. Pierre, *Variation et optimisation de formes: une analyse géométrique*. No. 48 in Mathématiques & applications, Berlin Heidelberg New York: Springer, 2005.

[16] G. Allaire and M. Schoenauer, *Conception optimale de structures*, vol. 58. Springer, 2007.

[17] M. Dambrine and K. Vyacheslav, "Robust obstacle reconstruction in an elastic medium," 2022.

[18] F. Hecht, O. Pironneau, A. Le Hyaric, and K. Ohtsuka, "Freefem++ manual," 2005.